JTTEE5 17:221–227
DOI: 10.1007/s11666-007-9145-1
1059-9630/$19.00 © ASM International 2007

Rare Earth/Metal Composite Formation by Cold Spray

Peter C. King, Saden H. Zahiri, and Mahnaz Z. Jahedi

(Submitted April 20, 2007; in revised form July 31, 2007)

$Nd_2Fe_{14}B$ permanent magnet/aluminum composite coatings were produced by cold spray deposition. Isotropic $Nd_2Fe_{14}B$ powder was blended with aluminum powder to make mixtures of 20-80 vol.% $Nd_2Fe_{14}B$, and these mixtures were sprayed at temperatures of 200-480 °C. The hard $Nd_2Fe_{14}B$ particles tended to fracture and fragment upon impact, while aluminum underwent severe plastic deformation, eliminating pores, and trapping $Nd_2Fe_{14}B$ within the coating. It was found that higher spray temperatures and finer $Nd_2Fe_{14}B$ particle sizes improved the retention rate of $Nd_2Fe_{14}B$ within the composite structure. This was explained from a contact mechanics viewpoint by calculating the effect of process parameters on the rebound momentum of $Nd_2Fe_{14}B$ particles. The magnetic properties of $Nd_2Fe_{14}B$ remained unaffected by the cold spray process.

Keywords cold gas dynamic spray, composite, magnetic properties, rare earth, rebound

1. Introduction

Cold gas dynamic spray, or simply cold spray, has emerged as a useful technology for the production of high-density metallic coatings without the problems associated with thermal spray techniques such as oxidation and thermal stresses. Cold spray of magnetic materials is one of the more intriguing possibilities. Iron itself is readily cold-sprayable (Ref 1). The idea of using spray technology to produce magnetic components for electronics applications, electric motors and the like, has been mentioned previously (Ref 2). Complex geometries can be built up directly on the substrate, with minimal post-machining operations. Other potential devices include sensors, magnetic couplings, and actuators.

High-energy rare earth permanent magnets, such as samarium-cobalt and neodymium-iron-boron alloys, have been the subject of considerable attention in recent years. These materials can be plasma-sprayed, but the resulting coating exhibits porosity, oxidation, and degradation of magnetic properties (Ref 3, 4). Rare earth permanent magnets are hard and brittle, so cold spray requires the magnetic powder to be mixed with a ductile metallic powder and the two sprayed together to form a metal matrix composite. Upon impact with the substrate, the metal matrix particles plastically deform extensively, eliminating pores and trapping the rare earth particles before they rebound. Van Steenkiste (Ref 5) has demonstrated the potential of the kinetic spray process for depositing composite coatings employing the rare earth magnetostrictive material, Terfenol-D. Rare earth permanent magnet composites have been produced using cold spray by McCune. The matrix material was a soft ferromagnetic metal such as iron or nickel (Ref 6). By contrast, in the current study, a non-magnetic matrix was chosen so that the effect of cold spray on the magnetic properties of the rare earth powder could be assessed independently without the additional complication of a second magnetic phase.

Generally speaking, there are two routes to cold spray production of composite coatings; either a blend of two powders can be sprayed as just described, or a single powder source of composite particles may be used, produced by the agglomeration of very fine particles of the two material components. The second approach has been used to cold spray nanocomposites (Ref 7, 8). However, the first technique, which is the focus of this investigation, requires an understanding of how to simultaneously spray two different types of particles, which may have different size distributions, morphologies, densities, and mechanical properties. The mechanics of composite formation, especially how hard particles become trapped in the coating and how cold spray and particle parameters affect this process, have been given little attention in the literature.

It is known for cold spray of single powder sources that there exists a critical velocity, above which particle bonding and coating formation are possible. The critical velocity depends on the thermal and mechanical properties of the material under question, notably its ability to deform easily, and to undergo localized adiabatic shearing (Ref 9, 10). One can consider cold spray of ductile metal/Nd-Fe-B combinations as representing an ideal case, where one component deforms considerably and deposits efficiently above its characteristic critical particle velocity, while the other exhibits effectively zero permanent

Peter C. King, Saden H. Zahiri, and **Mahnaz Z. Jahedi**, CSIRO Materials Science and Engineering, Gate 5, Normanby Road, Clayton, VIC 3168, Australia. Contact e-mail: Peter.King@csiro.au.

deformation. Raising the gas stagnation temperature increases the particle velocity of both components to varying degrees, and also causes some thermal softening of the ductile component. On its own, the deposition efficiency of the ductile component therefore increases with gas temperature. On the other hand, since the hard component can never be expected to reach its critical velocity within the range of experimental conditions investigated here, it will operate under an erosive regime: erosion of the coating material competes with the process of coating build-up.

Shkodin et al. (Ref 11) found that inclusion of a ceramic component in the powder mixture also causes a continuous activation of the surface which actually aids the metal deposition process. Increasing the ratio of ceramic to metal in the powder mix therefore yields higher deposition efficiencies of the pure metal component. The overall deposition efficiency of the powder mixture also increases initially with increasing ceramic content, but then reaches an optimum value and finally declines due to the lowering volume fraction of the metal component.

Cold spray tungsten/copper composites have been the subject of several studies. Shin et al. (Ref 12) studied the effect of temperature and relative particle size distribution on deposition efficiency and coating composition. However, with sufficient particle preheating tungsten shows some ability to deform upon impact, so that in this system the effect of process parameters on deformation of the hard phase has to be taken into account.

In the current investigation, cold spray deposition was utilized to fabricate $Nd_2Fe_{14}B$/aluminum composites. The $Nd_2Fe_{14}B$ particles showed no sign of permanent deformation, however tended to fracture, which complicated the analysis. The study focuses on the final composition of the coating compared to that of the starting powder mixture, rather than on deposition efficiency, as a measure of the $Nd_2Fe_{14}B$ particle retention rate.

2. Experimental Procedure

Inert gas atomized $Nd_2Fe_{14}B$ powder was supplied by Magnequench International, Inc. (MQP S-11-9) (Ref 13). The powder exhibits a fine particle size (median 33-55 μm, according to the supplier) making it suitable for cold spray, and a spherical morphology. The chemical composition was 15-22 wt.% Nd, 0-5 wt.% Pr, 0.5-1.8 wt.% B, 70-82 wt.% Fe, 0-5 wt.% Co, 0-5 wt.% Zr, and 0-5 wt.% Ti. The aluminum powder composition was min. 99.70% Al, and the median particle diameter was 21.3 μm. These two powders were mixed to give $Nd_2Fe_{14}B$ volume fractions from 20 to 80%. In some cases, a certain size fraction of the $Nd_2Fe_{14}B$ powder was separated out using a 20 or 38 μm sieve and mixed with the aluminum, in other cases the $Nd_2Fe_{14}B$ powder was not sieved.

The powder mixtures were sprayed using a CGT Kinetiks® 3000 cold spray system. Particles were fed from a powder feeder into a heated N_2 gas stream and accelerated through a conical converging-diverging (de Laval) nozzle. The powder in the feeder was heated to drive off any moisture, and mechanically agitated to separate the particles. The gas pressure and temperature in the nozzle prechamber were preset to 26 bar and 200-480 °C, respectively. The nozzle was aimed perpendicularly at aluminum alloy 5083 substrates from a standoff distance of 20 mm. An X-Y raster pattern, with a traverse speed of 200 cm/min, was traced repeatedly over a 20×25 mm area of the substrate. Coatings of at least several millimeters' thickness were built up. There was no sign of any tendency of the composite coatings to delaminate. For operation as a permanent magnet the coatings would normally require post-deposition magnetization using a high-strength magnetic field; however, since our samples were to undergo magnetic hysteresis measurement, this step was unnecessary.

Polished cross sections of the coatings were prepared by standard metallographic techniques. The volume fraction of retained $Nd_2Fe_{14}B$ was calculated by digital image analysis of optical micrographs of area 660×880 μm, and the final value for each coating was taken as an average of three such measurements. Specimens were cut from the coatings and fixed with epoxy resin in 8×5 mm (diameter) capsules. Magnetic hysteresis loops were measured using a Vibrating Sample Magnetometer (VSM) with the coating material oriented either perpendicular or parallel to the applied field.

3. Results

Figure 1 shows the volume fraction of retained $Nd_2Fe_{14}B$ in the coating determined by metallographic image analysis, as a function of temperature, for several $Nd_2Fe_{14}B$ volume fractions in the powder mixture and $Nd_2Fe_{14}B$ particle sizes. The data points for each powder mixture series were fitted using a quadratic function. The mixture employing +38 μm $Nd_2Fe_{14}B$ produced somewhat

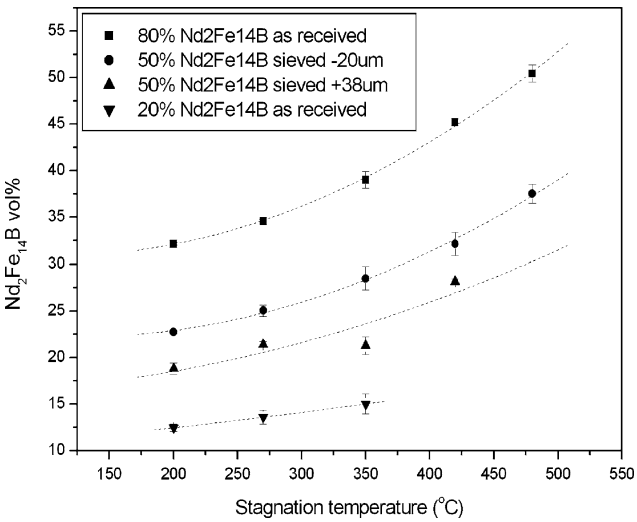

Fig. 1 Volume fraction of retained $Nd_2Fe_{14}B$ as a function of temperature for various powder mixtures

erratic results, probably due to the larger difference in mass distribution of the two components. The other mixtures showed a clear correlation between stagnation temperature and $Nd_2Fe_{14}B$ retention. A maximum concentration of 50 vol.% $Nd_2Fe_{14}B$ was achieved using the 80 vol.% powder mixture, although as a fraction of the original powder $Nd_2Fe_{14}B$ vol.%, higher powder concentrations yielded lower $Nd_2Fe_{14}B$ retention in the coating.

Microstructures of the composite deposits showed that many $Nd_2Fe_{14}B$ particles, but not all, had fractured (Fig. 2). The number of unbroken $Nd_2Fe_{14}B$ particles became less as higher concentrations of $Nd_2Fe_{14}B$ in the powder feedstock were used, due to a greater frequency of $Nd_2Fe_{14}B$-on-$Nd_2Fe_{14}B$ impacts. The extent to which individual particles were fragmented was also greater at higher $Nd_2Fe_{14}B$ concentrations. Small fragments and large unbroken particles alike were trapped and completely surrounded by the aluminum matrix. There was no evidence of any unfilled volume in the coatings, apart from missing pieces of $Nd_2Fe_{14}B$ which fell out during polishing of metallographic specimens.

The magnetic characteristics of coatings produced at three different temperatures are compared with the original 50% $Nd_2Fe_{14}B$ powder mixture in Fig. 3. The shape of the curves and the coercivity, H_{ci}, were unaffected by the cold spray process. The saturation magnetization fell in accordance with the lower volume fraction of $Nd_2Fe_{14}B$ in the coatings sprayed at lower temperatures (i.e., the magnetization per mass of $Nd_2Fe_{14}B$ was constant from sample to sample). There was no evidence that the brief exposure of the $Nd_2Fe_{14}B$ particles to elevated temperatures or their fracture upon impact altered their magnetic properties. The coating samples were measured both perpendicular and parallel to the spray direction; however, the results produced were identical. The maximum field available in the VSM was 2.0 T, and given the high intrinsic coercivity of the samples they may not have been fully saturated, and the loops may to a small extent be only minor ones.

The mechanism of $Nd_2Fe_{14}B$ entrapment in the coating depends on the nature of the $Nd_2Fe_{14}B$ impacts. In order to further investigate the $Nd_2Fe_{14}B$ particle impact process, $Nd_2Fe_{14}B$ powder was sprayed unmixed onto a cold-sprayed aluminum surface. In this way, the adhered $Nd_2Fe_{14}B$ particles could be observed without allowing a coating to build-up. The surface prior to $Nd_2Fe_{14}B$ deposition (Fig. 4a), which was similar to that encountered by the $Nd_2Fe_{14}B$ particles during composite coating, was very rough, with deep depressions in which the $Nd_2Fe_{14}B$ particles could well become lodged.

When $Nd_2Fe_{14}B$ was sprayed onto the cold-sprayed aluminum at a stagnation temperature of 200 °C, the surface was greatly altered (Fig. 4b). Most of the $Nd_2Fe_{14}B$ particles rebounded, leaving behind empty craters. Greater contrast between the aluminum and $Nd_2Fe_{14}B$ was achieved from backscattered imaging (Fig. 4c). Here, the occasional $Nd_2Fe_{14}B$ particle could be seen adhered to the surface. There were some particles that embedded into the aluminum, penetrating deeply below the surface. This type of phenomenon is commonly

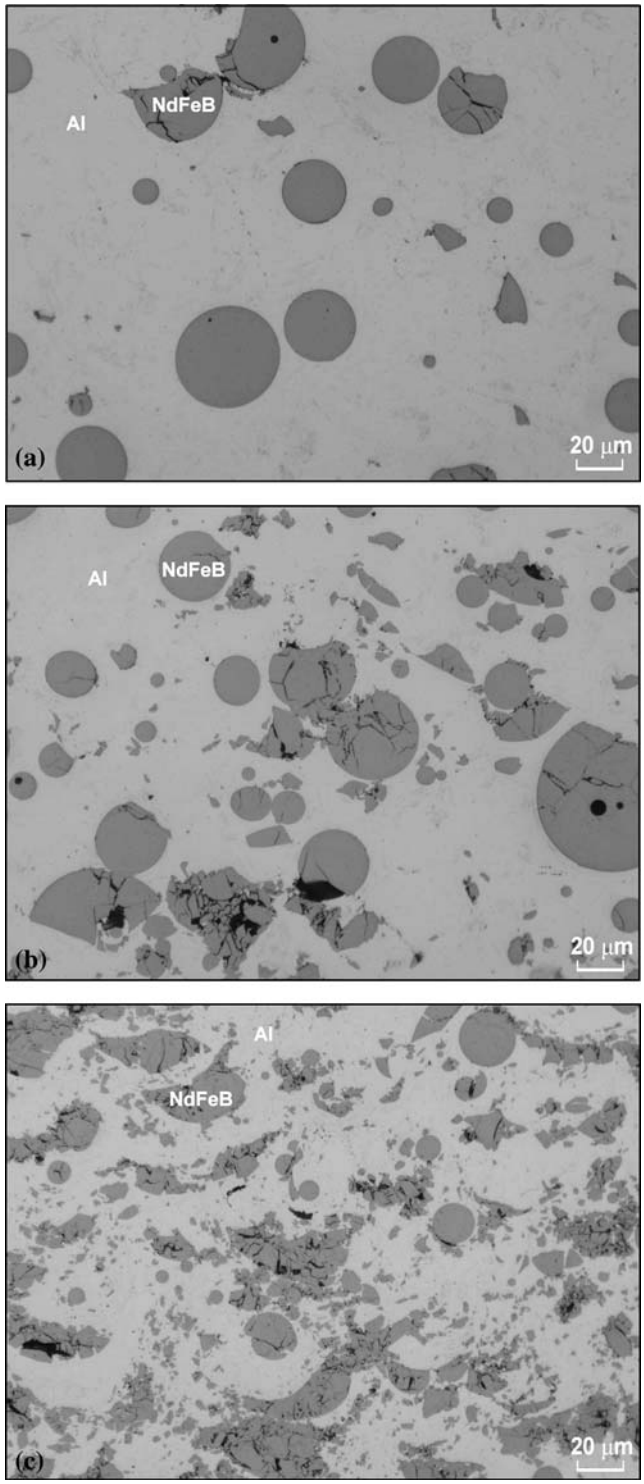

Fig. 2 Coating microstructures produced from various powder mixtures sprayed at 350 °C. (a) 20% $Nd_2Fe_{14}B$, (b) 50% $Nd_2Fe_{14}B$, and (c) 80% $Nd_2Fe_{14}B$

seen when a denser material is cold sprayed onto a lighter one (Ref 14), and is indicative of viscous flow of the matrix under sudden loading, due to highly localized heating at the interface. There was also a light covering of small

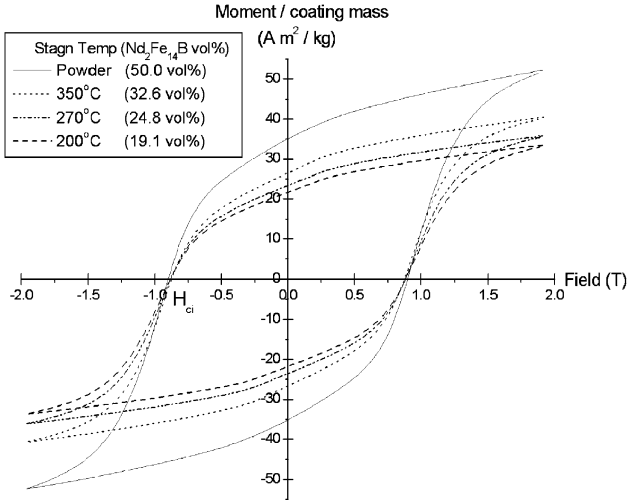

Fig. 3 Hysteresis loops for three cold spray coatings and the starting powder mixture, measured by VSM

fragments of $Nd_2Fe_{14}B$ particles that had been pressed into surface. However, at 100% $Nd_2Fe_{14}B$ concentration, and without any coating build up to cover the deposited $Nd_2Fe_{14}B$ particles, it was expected that this effect would be exaggerated by a greater degree of $Nd_2Fe_{14}B$-on-$Nd_2Fe_{14}B$ impact and fracture. The covering of the surface by fragmented material was even more apparent when $Nd_2Fe_{14}B$ was sprayed at 480 °C (Fig. 4d and e). Otherwise the two specimens were similar. Under both spray conditions, particle penetration and embedding were present; however, the ratio of adhered particles to empty craters was very low, and it was not measurably improved by increasing the $Nd_2Fe_{14}B$ impact velocity. Hence, when aluminum and $Nd_2Fe_{14}B$ are sprayed together, $Nd_2Fe_{14}B$ particles are mainly retained in the coating via entrapment by later-arriving aluminum particles, which deform, and surround the $Nd_2Fe_{14}B$.

4. Discussion

In order to understand how particle size distribution and impact velocity influence the retention of $Nd_2Fe_{14}B$ particles in the final coating, we can consider the impact of a single $Nd_2Fe_{14}B$ particle on the coating surface during the build-up of the composite coating. The problem is essentially one of a rigid, elastic sphere impacting against a deformable plane. The particle will rebound off the surface unless its momentum is small enough for it to be immobilized by later-arriving particles and retained in the coating. This situation is illustrated in Fig. 5. Here we assume that the jet particle loading was sufficiently low that clustering en route to the substrate can be ignored. Hence, individual particles impact the substrate independently.

The $Nd_2Fe_{14}B$ particle may strike an area of the coating containing either aluminum or $Nd_2Fe_{14}B$. In the former case, the $Nd_2Fe_{14}B$ particle and the aluminum will initially deform elastically as the center of mass of the particle draws closer to the coating surface. However, the yield limit of the aluminum will quickly be exceeded and a mixed elastic/plastic regime comes into effect. Since during high-speed impact there is limited time for the heat generated by friction and plastic deformation to dissipate, the effect of thermal softening on the mechanical properties of the aluminum cannot be neglected. Thermal softening causes a localization of strain near the particle interface, and may lead to a complete local breakdown in stress, or adiabatic shear instability. Thus deformation of the aluminum during deceleration of the $Nd_2Fe_{14}B$ particle is a complicated, dynamic process that can incorporate some viscous-like behavior. Ultimately, due to elastic forces, the center of mass of the $Nd_2Fe_{14}B$ particle starts moving in the opposite direction, away from the coating, and eventually the particle loses contact with the surface. If the $Nd_2Fe_{14}B$ impacts $Nd_2Fe_{14}B$ in the coating, the impact will be more elastic in nature.

In any one of these scenarios, we can define the contact time, t_c, as the period from the time the $Nd_2Fe_{14}B$ particle reaches the coating surface to the time that it loses contact. Its velocity at the moment it loses contact, when the elastic energy stored during impact is fully released kinematically, determines the total momentum that must be overcome by later-arriving particles during the time t_c.

The total momentum of later-arriving aluminum and $Nd_2Fe_{14}B$ particles that is required to trap the rebounding particle is given by Eq 1.

$$\sum m_{Al}u_{Al} + \sum m_{Nd_2Fe_{14}B}u_{Nd_2Fe_{14}B} \geq m_r u_r \qquad \text{(Eq 1)}$$

where m_r = mass of the rebounding particle, u_r = velocity of the rebounding particle at the moment that it loses contact with the surface, m_{Al} = mass of later aluminum particle, u_{Al} = velocity of later aluminum particle, $m_{Nd_2Fe_{14}B}$ = mass of later $Nd_2Fe_{14}B$ particle, and $u_{Nd_2Fe_{14}B}$ = velocity of later $Nd_2Fe_{14}B$ particle.

If the rebounding particle breaks up into a number, n, of fragments during impact, then the right-hand side term may be replaced by $\sum_{i=1}^{n} m_i u_i$, whose value, from conservation of momentum, cannot nevertheless exceed that of the parent particle, $m_r u_r$. From a simple isentropic gas flow model (Ref 15), it can be shown that increasing stagnation temperature has a greater bearing on the nozzle exit velocity of lighter particles (u_{Al}) than on heavier particles ($u_{Nd_2Fe_{14}B}$ and u_r), Fig. 6.

Most importantly, when the average velocity of all particles is raised, the right-hand side of Eq 1 does not increase correspondingly, due to energy loss via a number of inelastic processes that occur during the collision. The velocity u_r, of the rebounding particle is related to its pre-impact velocity u_0 via the coefficient of restitution η, where $\eta = 1$ represents an ideally elastic collision.

$$\eta = \frac{u_r}{u_0} \qquad \text{(Eq 2)}$$

There have been many studies of the relationships between η, particle size, and velocity of impact. Overall, η decreases with u_0 as the collision becomes increasingly inelastic. However, the results vary greatly depending on the exact

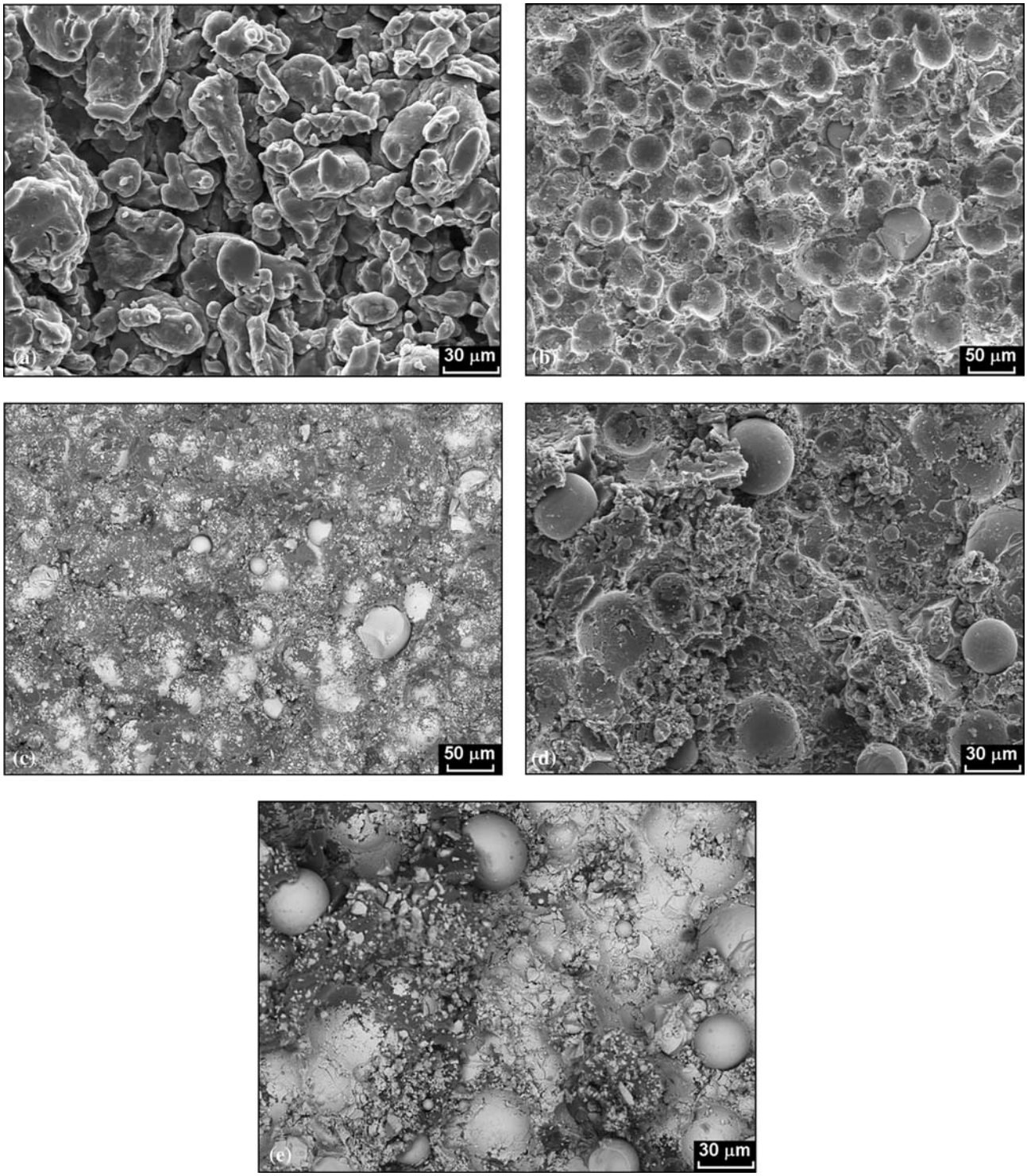

Fig. 4 (a) As-deposited aluminum cold spray surface. (b, c) Following exposure to cold sprayed $Nd_2Fe_{14}B$ particles at 200 °C stagnation temperature; (b) SE image, (c) backscattered image. (d, e) Following exposure to cold sprayed $Nd_2Fe_{14}B$ particles at 480 °C stagnation temperature; (d) SE image, (e) backscattered image

system under scrutiny and η may not even be a monotonic function of u_0 (Ref 16, 17). Viscoplastic flow of aluminum in the coating surface is a major energy loss mechanism, which becomes more significant with increasing impact velocity and penetration (Ref 18). Fracture and/or fragmentation of the impacting particle is also an inelastic process, for which $\eta \rightarrow 0$ as velocity increases (Ref 19).

Any adhesive interaction, even if only dispersion forces, between the particle and the coating must also be taken into account. Although below the critical velocity

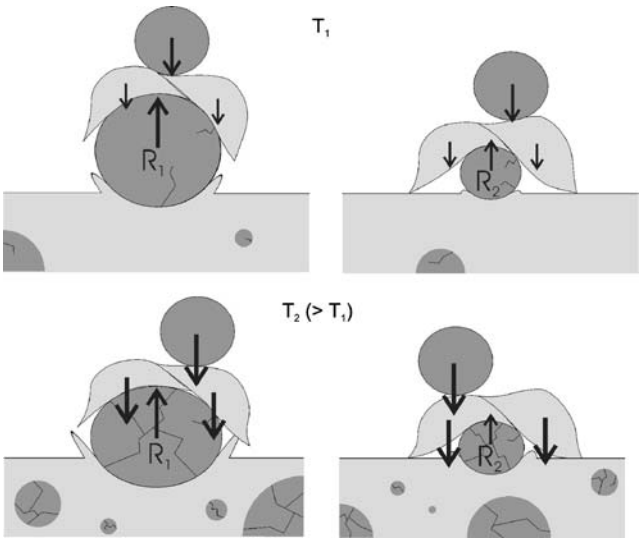

Fig. 5 Rebound of a $Nd_2Fe_{14}B$ particle (dark) from the coating surface and capture by later-arriving aluminum (light) and $Nd_2Fe_{14}B$ particles. The momentum of each particle is indicated by the size of the vector drawn from its center of mass. The relative momentum of the particles shifts in favor of the aluminum particles with an increase in spray temperature from T_1 (top) to T_2 (bottom), and a decrease in rebounding $Nd_2Fe_{14}B$ particle size from R_1 (left) to R_2 (right). The extent of fracture of the rebounding $Nd_2Fe_{14}B$ particle, penetration into the substrate and degree of substrate shearing are also illustrated

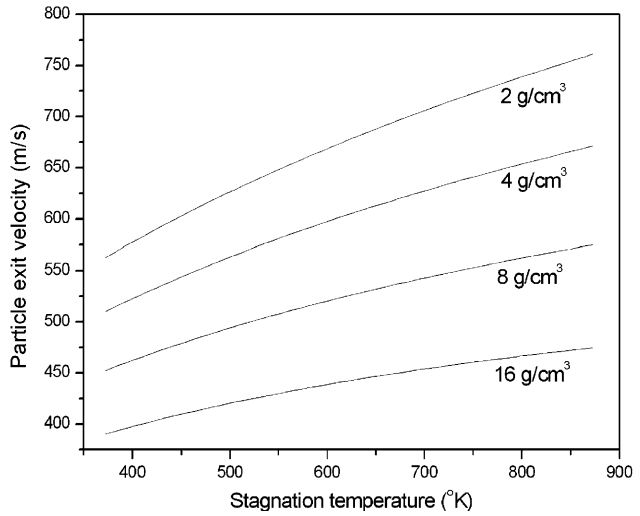

Fig. 6 Effect of temperature on particle velocity at the nozzle exit for 20-μm diameter particles of various densities

for cold spray deposition, adhesion during grit-blasting processes is occasionally strong enough to cause some particles to stick to the surface (Ref 20).

Hence, raising the stagnation temperature increases the left-hand side of Eq 1, but does not lead to a proportionate increase in the momentum of the rebounding particle. The net result is increasing $Nd_2Fe_{14}B$ entrapment, as seen in Fig. 1.

The effect of shifting the $Nd_2Fe_{14}B$ particle size distribution without altering that of the aluminum powder can also be explained in terms of rebound momentum. If larger $Nd_2Fe_{14}B$ particles are used, then $m_r u_r$ is greater because m_r depends strongly on the radius, $m_r = (4/3)\rho\pi r^3$. On the other hand, u_r will be lower because larger particles are more difficult to accelerate through the nozzle. Nevertheless, it can easily be shown that the dependence of u_0 (and therefore indirectly u_r) on r is not as great as that of m_r. Equation 3 relates the drag force on the particle-to-particle acceleration through the nozzle (Ref 15).

$$m\frac{du_p}{dt} = mu_p\frac{du_p}{dx} = \frac{C_D A_p \rho_g (u_g - u_p)^2}{2} \qquad \text{(Eq 3)}$$

where u_p = particle velocity, u_g = gas velocity, C_D = particle drag coefficient, A_p = cross-sectional area of particle, and ρ_g = gas density.

Impact velocity, u_0, can be taken to be roughly equal to u_p calculated by Eq 3, ignoring the effect of shock waves in the jet. Dykhuizen and Smith (Ref 15) found the following solution to Eq 3 by assuming gas velocity, density, and drag coefficient to be constant.

$$\log\left(\frac{u_g - u_p}{u_g}\right) + \frac{u_g}{u_g - u_p} - 1 = \frac{3C_D\rho_g x}{8\rho_p r} \qquad \text{(Eq 4)}$$

For $u_p \ll u_g$ this simplifies to:

$$u_p = u_g\sqrt{\frac{3C_D\rho_g x}{4\rho_p r}} \qquad \text{(Eq 5)}$$

Thus u_p goes approximately as $r^{-1/2}$ whereas m depends on r^3, with the net result that larger $Nd_2Fe_{14}B$ particles have greater momentum and are more difficult to trap in the coating, as seen in Fig. 1.

It is known that when brittle particles impact a surface, a threshold velocity exists for fracture. This threshold velocity decreases with particle size (Ref 19, 21). It might then be expected that by limiting the $Nd_2Fe_{14}B$ particle size, fracture will be avoided. However, in our experiments with $Nd_2Fe_{14}B$ powder sieved to −20 μm, fracture was just as prevalent as with +38 μm powder. In fact, when finer particles are used, there is competition between the higher threshold velocity for fracture, and greater particle acceleration through the nozzle. It is hoped that future experiments on a greater range of particle sizes might find the right conditions under which fracture is eliminated.

It is interesting to note that while decreasing $Nd_2Fe_{14}B$ particle size or increasing particle acceleration shifts the momentum balance toward greater $Nd_2Fe_{14}B$ retention by successive impacts, the time in which this occurs is actually less. The contact time of a spherical particle during impact against a plane can be calculated from Hertz contact theory (Ref 16, 22). If the plane deforms only elastically, the contact time t_e, of a particle of radius r, density ρ, and impact velocity u_0, is given by the following expression.

$$t_e = 1.47\left(\frac{5\pi}{4}\right)^{2/5} r\left(\frac{\rho^2 E^{*2}}{u_0}\right)^{1/5} \quad \text{(Eq 6)}$$

where

$$\frac{1}{E^*} = \frac{(1-\nu^2_{particle})}{E_{particle}} + \frac{(1-\nu^2_{plane})}{E_{plane}} \quad \text{(Eq 7)}$$

E = elastic modulus, and υ = Possion's ratio.

However, it is known that above the yield stress, the deformation process changes from elastic to plastic. For purely plastic deformation, the contact time t_p is determined from Eq 8.

$$t_p = \frac{\pi}{2} r\left(\frac{2\rho}{3P_d}\right)^{1/2} \quad \text{(Eq 8)}$$

where P_d is the flow pressure.

In practice, deformation is mixed, and both elastic and plastic terms contribute to the total contact time. In both Eq 6 and 8, the residence time of $Nd_2Fe_{14}B$ particles on the surface increases linearly with r. The elastic contact time also decreases with increasing particle velocity, while t_p is independent of u_0.

5. Conclusions

We have found that hard magnetic particles may be cold sprayed simultaneously with a ductile matrix material to form a composite coating, without compromising magnetic properties. Over the range of particle velocities that were studied, a small proportion of $Nd_2Fe_{14}B$ particles were able to penetrate deeply into aluminum. However, the remaining particles, which would otherwise have rebounded elastically from the surface, were retained in the coating if their rebound momentum was small enough to be overcome by later-arriving particles. This explained the observed results that $Nd_2Fe_{14}B$ retention increased with increasing stagnation temperature and with smaller $Nd_2Fe_{14}B$ particle sizes.

Acknowledgments

The authors would like to thank Dr Stephen Collocott and Dr John Dunlop from CSIRO Industrial Physics for performing the VSM measurements.

References

1. R.C. McCune, R.P. Cooper, and O.O. Popoola, Post-processing of Cold-spray Deposits of Copper and Iron, *Thermal Spray Surface Engineering via Applied Research: Proceedings of the 1st International Spray Conference*, C.C. Berndt, Ed. (Montreal, Canada), ASM International, 2000, p 905-908
2. U. Varshney, B.D.I. Eichelberger, J.A.I. Neal, R.J. Churchill, K.D.T. Ngo, and R.J. Thibodeaux, Monolithic Magnetic Modules for Aerospace Power Electronics, *Energy Conversion Engineering Conference, 1997. IECEC-97. Proceedings of the 32nd Intersociety*, 1997, p 370-374
3. K. Kumar, D. Das, and E. Wettstein, Samarium-cobalt Magnets Resistant to 750C, *IEEE Trans. Magn.*, 1978, **14**(5), p 788-790
4. R.A. Overfelt, C.D. Anderson, and W.F. Flanagan, Plasma Sprayed $Fe_{76}Nd_{16}B_8$ Permanent Magnets, *Appl. Phys. Lett.*, 1986, **49**(26), p 1799-1801
5. T. Van Steenkiste, Kinetic Sprayed Rare Earth Iron Alloy Composite Coatings, *Thermal Spray 2006: Science, Innovation, and Application*, B.R. Marple and C. Moreau, Eds. (Seattle, USA), ASM International, 2006
6. R.C. McCune, Potential Applications of Cold-spray Technology in Automotive Manufacturing, *Thermal Spray 2003: Advancing the Science and Applying the Technology*, C. Moreau and B. Marple, Eds., ASM International, 2003, p 63-70
7. H.-J. Kim, C.-H. Lee, and S.-Y. Hwang, Superhard Nano WC-12%Co Coating by Cold Spray Deposition, *Materi. Sci. Eng. A*, 2005, **391**(1-2), p 243-248
8. R.S. Lima, J. Karthikeyan, C.M. Kay, J. Lindemann, and C.C. Berndt, Microstructural Characteristics of Cold-sprayed Nanostructured WC-Co Coatings, *Thin Solid Films*, 2002, **416**(1-2), p 129-135
9. T. Schmidt, F. Gartner, H. Assadi, and H. Kreye, Development of a Generalized Parameter Window for Cold Spray Deposition, *Acta Mater.*, 2006, **54**(3), p 729-742
10. H. Assadi, F. Gartner, T. Stoltenhoff, and H. Kreye, Bonding Mechanism in Cold Gas Spraying, *Acta Mater.*, 2003, **51**(15), p 4379-4394
11. A. Shkodkin, A. Kashirin, O. Klyuev, and T. Buzdygar, Metal Particle Deposition Simulation by Surface Abrasive Treatment in Gas Dynamic Spraying, *J. Therm. Spray Technol.*, 2006, **15**(3), p 382-386
12. S. Shin, S. Yoon, Y. Kim, and C. Lee, Effect of Particle Parameters on the Deposition Characteristics of a Hard/Soft-particles Composite in Kinetic Spraying, *Surf. Coat. Technol.*, 2006, **201**(6), p 3457-3461
13. B.M. Ma, J.W. Herchenroeder, B. Smith, M. Suda, D.N. Brown, and Z. Chen, Recent Development in Bonded NdFeB Magnets, *J. Magn. Magn. Mater.*, 2002, **239**(1-3), p 418-423
14. V.K. Champangne, D. Helfritch, P. Leyman, S. Grendahl, and B. Klotz, Interface Material Mixing Formed by the Deposition of Copper on Aluminium by means of the Cold Spray Process, *J. Therm. Spray Technol.*, 2005, **4**(3), p 330-334
15. R.C. Dykhuizen and M.F. Smith, Gas Dynamic Principles of Cold Spray, *J. Therm. Spray Technol.*, 1998, **7**(2), p 205-212
16. I.M. Hutchings, Strain Rate Effects in Microparticle Impact, *J. Phys. D: Appl. Phys.*, 1977, **10**, p L179-L184
17. H. King, R. White, I. Maxwell, and N. Menon, Inelastic Impact of a Sphere on a Massive Plane: Nonmonotonic Velocity-dependence of the Restitution Coefficient, *ArXiv Condensed Matter e-prints*, 2002, 0209490
18. R. Ramirez, T. Poshel, N.V. Brilliantov, and T. Schwager, Coefficient of Restitution of Colliding Viscoelastic Spheres, *Phys. Rev. E*, 1999, **60**(4), p 4465-4472
19. M. Higa, M. Arakawa, and N. Maeno, Side Dependence of Restitution Coefficients of Ice in Relation to Collision Strength, *Icarus*, 1998, **133**(2), p 310-320
20. L.N. Rogers and J. Reed, The Adhesion of Particles Undergoing an Elastic-plastic Impact with the Surface, *J. Phys. D: Appl. Phys.*, 1984, **17**, p 677-689
21. E.W. Andrews and K.S. Kim, Threshold Conditions for Dynamic Fragmentation of Ceramic Particles, *Mechan. Mater.*, 1998, **29**(3-4), p 161-180
22. K.L. Johnson, Contact Mechanics. Cambridge University Press, Cambridge, Great Britain, 1985